

Research article

Chang Zhao, Lilong Dai, Qianqian Huang, Zinan Huang, Chengbo Mou*, Mohammed Al Araimi, Aleksey Rozhin, Sergey Sergeev and Zhichao Luo

Dynamic polarization attractors of dissipative solitons from carbon nanotube mode-locked Er-doped laser

<https://doi.org/10.1515/nanoph-2019-0508>

Received December 8, 2019; accepted January 31, 2020

Abstract: We report experimental observation of polarization attractors in the form of vector dissipative solitons from a carbon nanotube mode locked fiber laser. At a time scale of 14–14,000 roundtrips, the typical polarization locked vector solitons, and other appealing attractors are shown. In addition, we observe the vector dissipative solitons operated in dual-wavelength regime with central wavelength of 1533 and 1557 nm which can be related to a fixed point polarization attractor. The results unveiled complex oscillatory behavior of dissipative solitons in the polarization domain which may help understand laser physics, nonlinear optics. The demonstrated work may underpin a new type of high energy laser source leading to possible applications in nanoparticle manipulation, micromachining, spectroscopy etc.

Keywords: dissipative solitons; fiber laser; polarization attractors.

***Corresponding author: Chengbo Mou**, Key Laboratory of Specialty Fiber Optics and Optical Access Networks, Shanghai Institute for Advanced Communication and Data Science, Joint International Research Laboratory of Specialty Fiber Optics and Advanced Communication, Shanghai University, Shanghai, 200444, PR China, E-mail: mouc1@shu.edu.cn. <https://orcid.org/0000-0001-6107-3439>

Chang Zhao, Lilong Dai, Qianqian Huang and Zinan Huang: Key Laboratory of Specialty Fiber Optics and Optical Access Networks, Shanghai Institute for Advanced Communication and Data Science, Joint International Research Laboratory of Specialty Fiber Optics and Advanced Communication, Shanghai University, Shanghai, 200444, PR China

Mohammed Al Araimi: Higher College of Technology, Al-Khuwair, PO Box 74, Postal Code 133, Muscat, Oman

Aleksey Rozhin and Sergey Sergeev: Aston Institute of Photonic Technologies (AIP), Aston University, Birmingham, B4 7ET, UK

Zhichao Luo: Guangdong Provincial Key Laboratory of Nanophotonic Functional Materials and Devices, South China Normal University, Guangzhou, 510006, PR China

1 Introduction

Ultrashort pulses generated from fiber lasers have attracted tremendous attention of researchers and widely used in many fields such as optical communication, spectroscopy, biomedical imaging [1]. As a powerful tool, various attentions have been focused on the performance of ultrafast fiber laser such as average power, peak power, pulse duration, lasing wavelength and recently timing jitter. On the other hand, the vectorial nature of the ultrashort pulses suggests extra dimensionality of the pulse physical properties. Typical vector soliton (VS), whose pulse shaping mechanism resulting from the balance between dispersion and nonlinearity, has been widely explored in ultrafast fiber laser systems. These vector solitary waves usually contain two mutually coupled orthogonal polarization components with fixed, periodic evolved phase relationship or other more complex oscillatory behavior when propagating in the fiber. Recently there exists very intensive activities in 2D material mode-locked fiber lasers generating optical solitons [2–4]. VS can be now routinely generated from a passively mode locked fiber laser using artificial absorber rather than nonlinear polarization rotation mode locker with dynamic polarization patterns including polarization locked vector solitons (PLVSs) [5, 6], group velocity locked vector solitons (GVLVSs) [7, 8], polarization rotation vector solitons (PRVSs) [9, 10]. On the other hand, for a typical dissipative soliton (DS) pulse, the balance among non-linearity and dispersion, loss and gain is necessary to satisfy continuous energy exchange with the environment along with the redistribution of energy among different parts of soliton. By optimizing the cavity properties such as spectral filtering, nonlinearity and dispersion, wide range of profiles of dissipative solitons can be observed, offering abundant evolution of solitons. Due to the intrinsic nature of supporting high energy, the vector dissipative soliton (VDS) attracted much more attention since their appearance. It is observed that the dynamic evolution of DS also appears to be vectorial [11–14]. However, by far, the evolution of phase

difference between the two polarization components and degree of polarization (DOP) has been ignored leading no correlation to polarization attractors.

Here attractor is defined as an asymptotic state demonstrating the evolution of state of polarization (SOP) at different time scales involving various mechanisms. Recently, it is observed various types of attractors such as fixed point, limited cycle, spiral attractors and so forth could appear in the polarization domain with the format of trajectories on the surface of Poincare sphere exhibiting continuous variation of the SOP [15–22]. Such behavior can be related with the laser cavity anisotropy, gain and loss dynamics. It is therefore fundamentally interesting to explore the vectorial properties of DS, especially to the generation of polarization attractors.

In this paper, we report a systematic experimental study of novel types of VDS in terms of polarization attractors in a carbon nanotube mode locked DS fiber laser. Using a commercial polarimeter, we have successfully presented VDS with locked and precessing SOP for both single wavelength and dual wavelength DS on a time scale of 14 to 14,000 roundtrips from 1 μ s to 1 ms. The observed attractors may contribute to more in-depth understanding of nonlinear science, laser physics and underpin future laser technologies with versatile polarization control.

2 Characterization of CNT-PVA film and laser configuration

The preparation of saturable absorber (SA) has been demonstrated detailed in the literature [23]. Single walled

CNTs possess higher transparency when irradiated by higher optical power due to the excitonic transitions and has fast recovery time [24]. Owing to the optical saturable absorption of CNTs, self-started mode-locking can be readily achieved at a pump power of several tens milliwatts. What is more essential, randomly distributed CNTs in polymer matrix facilitate the polarization independency of SA so that support the VS generation in a mode locked fiber laser. The CNT-SA was characterized by both nonlinear transmission measurement and Raman spectroscopy as shown in Figure 1. From Figure 1A, the modulation depth, saturable intensity and non-saturable loss are 1.7%, 13.75 μ J/cm² and 61.96% respectively. Raman spectrum of CNT film obtained with the excitation light of 633 nm is indicated in Figure 1B. The clear G-band can be the proof of the existence of carbon atom because the peak is caused by the in-plane vibration of sp²-hybridization carbon. The split of G-band can be unambiguously attributed to the symmetry-breaking effects related to the curvature of CNT [25]. The D-band is generally used to measure the defect of CNT [26]. Apparently there exists little disorder or defects indicating high quality CNT-SA. The radial breathing mode (RBM) is used to characterize the nanotube diameter and chirality assignment [27]. We can assign the dominant diameters of our CNTs as 0.85, 0.96, 1.1, 1.25 nm and the range of diameter is about 0.77–1.36 nm [28].

Figure 1(C) demonstrates the schematic configuration of CNT-SA based passively mode locked fiber laser. 0.98 m erbium doped fiber (EDF, OFS EDF 80) as gain medium with a group velocity dispersion (GVD) of +66.1 ps²/km is incorporated in the cavity with total length of 14.52 m. We select 2 m dispersion compensation fiber (DCF) with a GVD

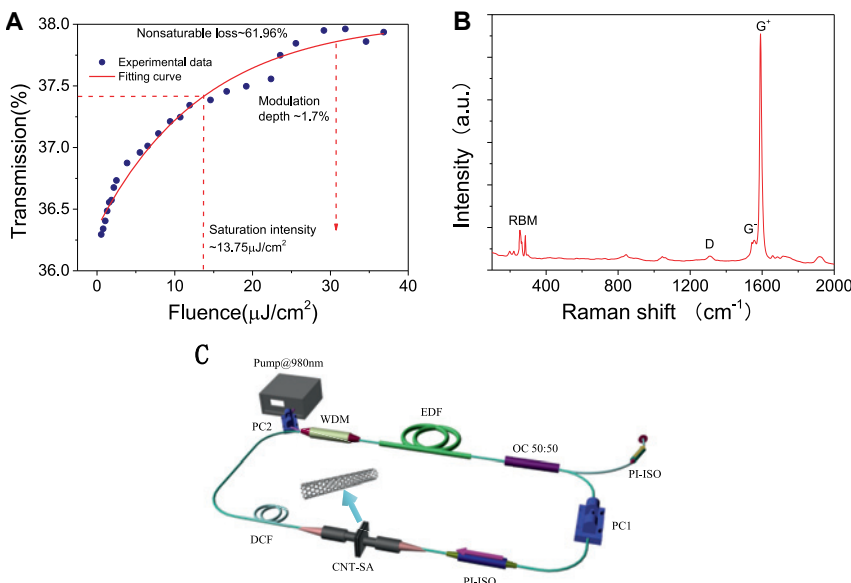


Figure 1: Characterization of CNT-PVA film. (A) The measured nonlinear transmission of CNTs-PVA film. (B) Raman spectrum of CNTs-PVA film under the excitation of 633 nm. (C) The schematic configuration of passively mode-locked all-fiber laser based on CNT-PVA film.

of $+163.96 \text{ ps}^2/\text{km}$ so that the laser can work in DS regime. In addition, the rest of fiber is SMF with an anomalous dispersion of $-22 \text{ ps}^2/\text{km}$. Consequently, the net dispersion of the cavity is 0.139 ps^2 , which is clearly pronounced for the DS generation. A 980 nm laser module (OV LINK) is utilized to supply pump light for EDF through a 980/1550 nm wavelength division multiplexer (WDM). Connected with EDF is a 50:50 optical coupler. We implement polarization controller (PC1) to tune the SOP in the cavity. An additional in-line PC2 was also used to adjust polarization of pump and optimize anisotropy in the cavity caused by birefringence and polarization dependent losses. The polarization independent isolator (ISO) possesses the capacity to guarantee the pulse transmit in a unidirectional manner. Besides, we laid an extra ISO outside the cavity to eliminate any possible reflection from the light existing out the cavity. The CNT-PVA film is incorporated in the cavity using two standard fiber connectors to act as a mode locker.

Pulse characteristics are identified by 8 GHz oscilloscope (KEYSIGHT DSO90804A) and 3.2GHz signal analyzer (SSA, 3032X) connected with 12.5 GHz photodetector (Newport 818-BB-51F). Pulse duration of the pulses can be identified by a commercial autocorrelator (FEMTOCHROME, FR-103WS). Optical spectrum can be observed utilizing an optical spectrum analyzer (OSA, Yokogawa AQ6370C) with a maximum resolution of 0.02 nm. Furthermore, a commercial polarimeter (THORLABS, IPM5300) is used to detect the SOP transition of the soliton pulses with $1 \mu\text{s}$ resolution and 1024 sampling rate. Consequently, 1 MH sampling rate is far less than the fundamental frequency, leading to the trajectories presented on Poincare sphere are averaged results. An

external fiber attenuator was employed between the laser and polarimeter in order to protect the detector within. Furthermore, it is noted that the pulse duration is far less than of the pulses interval, as a result, amplified spontaneous emission (ASE) will supply integral optical signal of polarimeter during the pulse interval. As the DOP of ASE is nearly zero, the integral DOP detected by photodetector must be less than 100%.

3 Experimental results and discussions

Under the pump power of 90 mW, self-started mode locking can be achieved straightforwardly because of the low mode-locked threshold of the CNT SAs. By increasing the pump power and appropriately adjusting PC in the cavity, stable DS can be easily obtained under the pump power of 140 mW, which can be proved by the typical rectangular-like optical spectrum with 7.11 nm spectral bandwidth shown in Figure 2A. The radio frequency (RF) spectrum over 3 GHz span with bandwidth of 1 kHz is shown in Figure 2B, indicating our pulses are stable under this operation regimes. The pulse train shown in inset is measured by the oscilloscope giving the pulse period of 71 ns, corresponding to the repetition of 14.1 MHz. The autocorrelation (AC) measurement results can be fitted using Gaussian shape with pulse duration of 30.41 ps as shown in Figure 2C. Figure 2D represents the averaged SOP on the Poincare sphere within 1 ms in the form of a fixed point. Figure 2E displays the output power of two orthogonal polarization components, giving stable evolving power. The reason that the power derived from polarimeter

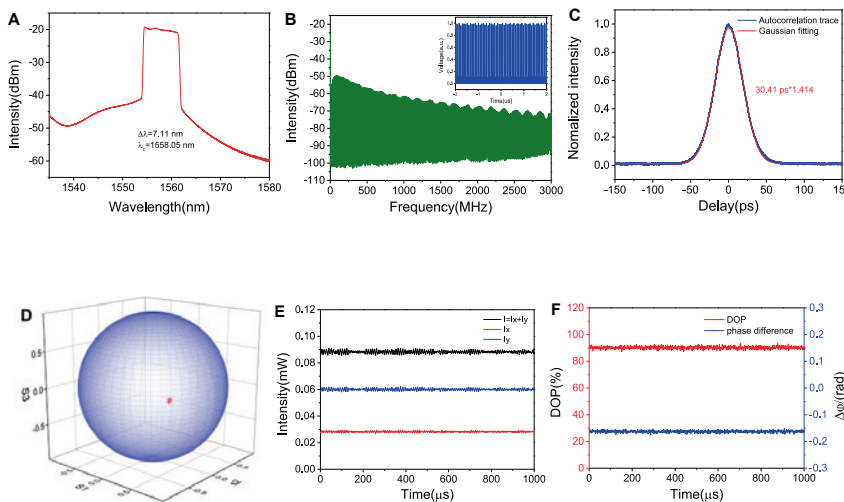


Figure 2: PLVDS generated under the pump power of 140 mW. (A) Typical DS Optical spectrum with resolution of 0.02 nm. (B) RF spectrum over 3 GHz span. The inset shows the pulse train visualized in oscilloscope. (C) Measured AC trace (blue line) and fitting AC trace (red line). (D) Normalized Stokes parameters shown by Poincare sphere. (E) Optical power of two cross-polarized SOPs. (F) DOP and phase difference.

measurement is much lower than real output is due to the settled attenuator between laser output coupler and polarimeter. Figure 2F shows clearly a fixed phase difference between two linear cross-polarized SOP, indicating the soliton is polarization locked vector dissipative soliton (PLVDS) caused by strong coupling between two crossed SOP. The measured point attractor is clearly located near the equator announcing the linear polarized light. However, this is due to the birefringence compensation through the leading fiber to the polarimeter, the output laser light is thus elliptical polarized. The stable SOP also indicates the high DOP of the VDS over a fixed period of time. The size of the trajectory on the Poincare sphere may be larger than the measured trace because of the averaged measurement. However, we can qualitatively estimate whether the trajectory is fixed point or not by DOP, which means the size of the trajectory covered area is inversely proportional to DOP. Consequently, high DOP illustrates that SOP for this case is evolving slowly and vice versa. This is because that the cavity becomes more anisotropic when the SOP of pump gets more elliptical, making the system approach a steady state in the form of PLVDS corresponding to fixed point shown on surface of Poincare sphere.

With the pump power increase to 180 mW, a standard DS was observed again as shown in Figure 3. Figure 3A shows the typical dissipative spectrum with tiny defect on the top left corner. Under the pump power of 180 mW, the bandwidth of spectrum is 8.87 nm, larger than that shown in Figure 2 and lead to a higher single pulse energy. Such spectral widening effect along pump power increase is a typical feature of DS [29]. Figure 3B and C shows very similar pulse characterization of RF spectrum, pulse train and AC trace compared with Figure 2B and C. Figure 3D demonstrates a semicircular trajectory, a complex oscillations accompanied by polarization jump between two

cross-polarized SOPs averaged over 14 pulses, which can be corroborated by the corresponding defected optical spectrum. This attractor demonstrates the switch between two orthogonal SOP. Figure 3E represents strong anti-phase dynamics of the two orthogonal components leading to oscillated output power. The period of relaxation oscillations shown in Figure 3E can be estimated with the rate of relaxation for population inversion in EDF and round-trip time [20]. Moreover, DOP and phase difference are shown by Figure 3F. Apparently, the phase between two cross-polarized SOP switches between $-3\pi/4$ and $\pi/4$ and the phase difference jumps at the position of very low DOP. Such intensity relaxation oscillation was previously observed in a VS laser with spiral polarization attractor [20]. For a spiral polarization attractor, relaxation oscillation was observed in both crossed SOP. We can therefore define a new type attractor here that only one of the cross-polarized SOPs exhibits power relaxation oscillations.

Further increasing the pump power to 190 mW and slightly adjusting PC, we obtain the DS optical spectrum without defect appeared in Figure 4A. RF spectrum, oscilloscope image and AC trace are shown in Figure 4B and C. Figure 4D illustrates an irregular trajectory on the Poincare sphere, which is similar to the trace shown in Figure 3D. However, most of the pulses appear to be localized within the two points at the equator of the Poincare sphere. Anti-phase dynamics of orthogonal electric fields result in quasi stable CW total output power. The periodicity of the switching and the unbalanced residence time of two orthogonal SOP shown in Figure 4E and F indicates the existence of polarization instability which can be explicated by polarization hole burning and pumping anisotropy. This means that pump light creates an orientational distribution of the population inversion and elliptical polarized pump light can produce cavity anisotropy. The

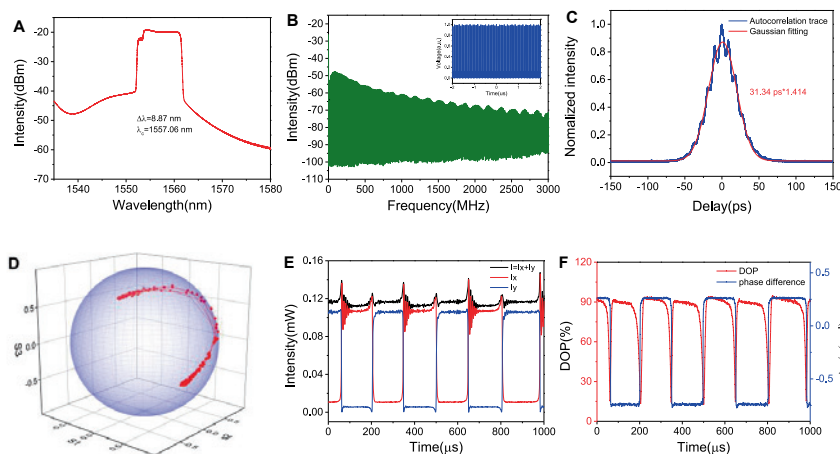


Figure 3: PLVDS with slowly evolving state of polarization under the pump power of 180 mW. (A) Typical DS Optical spectrum. (B) RF spectrum over 3 GHz span. The inset shows the pulse train visualized in oscilloscope. (C) Measured AC trace (blue line) and fitting AC trace (red line). (D) Normalized Stokes parameters shown by Poincare sphere. (E) Optical power of orthogonal component. (F) DOP and phase difference.

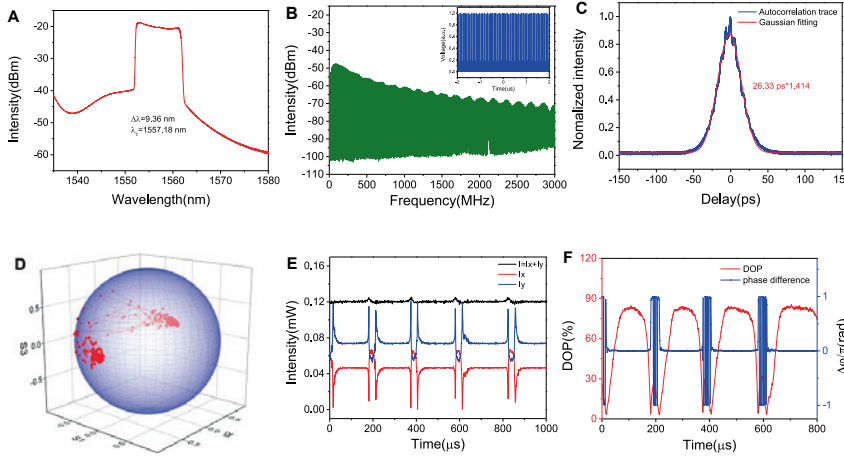


Figure 4: PLVDS with slowly evolving state of polarization under the pump power of 190 mW. (A) Typical DS Optical spectrum. (B) RF spectrum over 3 GHz span. The inset shows the pulse train visualized in oscilloscope. (C) Measured AC trace (blue line) and fitting AC trace (red line). (D) Normalized Stokes parameters shown by Poincare sphere. (E) Optical power of orthogonal component. (F) DOP and phase difference.

depth of a polarization hole strongly depends on the phase difference, resulting in coherent coupling of the two crossed SOP of solitons through gain sharing. Also, the depth is proportional to the lasing power, so the periodic oscillation of output power induces the periodic modulation of anisotropy of gain medium in the cavity.

When pump power increased up to 230 mW, we can obtain dual-wavelength operation with optical spectrum centered at 1557 and 1533 nm with the bandwidth of 3.2 and 9.2 nm respectively as shown in Figure 5A. Further increase the pump power to 300 mW, yielding the blue-shift of center wavelength of optical spectrum with bandwidth of 4.9 nm shown in Figure 5D. This is because the gain of EDF is proportional to the emission cross section when most of the population in the ground state are inverted to the upper state under the high optical power. Moreover, emission cross section for 1530 nm is higher than that for 1550 nm, which induces the evolution of gain of EDF with increasing the optical power. CW in Figure 5D can be explained by the incomplete population

inversion depletion through soliton pulses in each roundtrip. Unfortunately, no more other attractors can be found under the two operation regimes except for the PLVDSs owing to the strong coupling between two crossed SOP under the high optical power, corresponding to the fixed polarization attractor on the Poincare sphere shown in Figure 5B and E.

4 Conclusion

To the best of our knowledge, we firstly observe various types of attractors from the dimensionality of polarization in VDS regime from a CNTs mode-locked fiber laser on a time scale of 14–14,000 roundtrips, which demonstrate the coherent coupling between two orthogonal SOPs. We optimize cavity anisotropy through the cavity birefringence and pump light polarization state, bringing about the appearance of peculiar attractors. Except for the obtained standard PLVDS that indicates DS can work in a

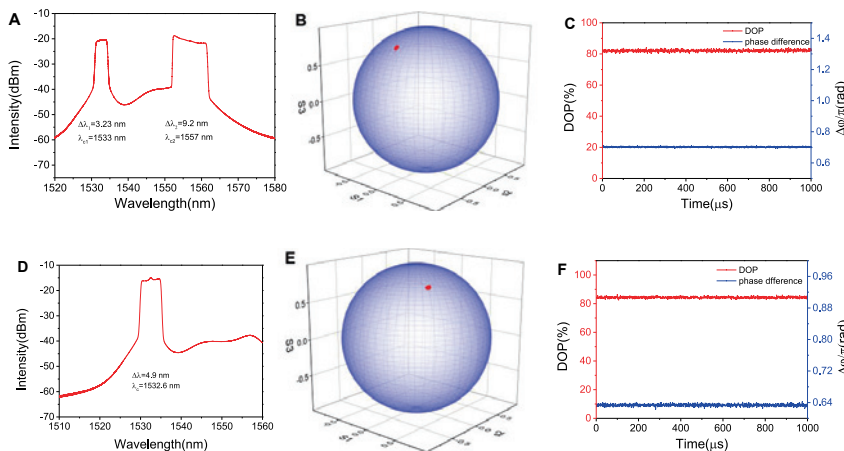


Figure 5: (A) and (D) Optical spectra of PLVDS under fixed pump power of 230 and 300 mW respectively. (B) and (E) PLVDSs shown on the Poincare sphere. (C) and (F) DOP and phase difference.

stable state, quasi-stable state can be also observed when SOP is in the form of periodic modulation of output power and can be proved by the unequal residence time of the two orthogonal crossed SOPs caused by polarization hole burning and pumping anisotropy. A distinct polarization attractor with power relaxation from only one of the orthogonal SOP has been observed for the first time. Fixed point polarization attractors have also been observed in the dual wavelength VDS regime as well. The absence of other dynamic polarization attractor under the dual wavelength VDS regimes is attributed to the increase of degree of coupling between two orthogonal SOPs. It is noted that other type of attractor such as limit cycle can be also observed. From the experimental results, we can observe that when optical spectrum, RF, ACF and pulse trains are stable, the SOP may not be. We experimentally confirmed that polarization is an extra dimension of the physical properties of ultrashort pulses in the DS regime which can lead to polarization attractors. The polarization attractors can be observed in the VDS regime. Without external perturbation, each type of obtained polarization attractors is stable and can be reproduced. The presented work may guide us to understand nonlinear dynamics in nanomaterials-based lasers and fundamental physics in the dissipative system, which may provide the possibility to explore a novel type of high energy ultrashort pulse lasers for the applications of spectroscopy [30], laser machining [31], nano particle manipulation [32] and valleytronics [33] etc. In the future, polarimeter with higher timing resolution that equals to the roundtrip time is required to interpret pulse to pulse dynamics more accurately.

Acknowledgments: National Natural Science Foundation of China (NSFC) (61605107, 61975107); the Open Fund of IPOC2017B010 (Beijing University of Posts and Telecommunications, BUPT) and Open fund of Guangdong Provincial Key Laboratory of Functional Nanophotonic Materials and Devices, South China Normal University, Guangzhou, China; Young Eastern Scholar Program at Shanghai Institutions of Higher Learning (QD2015027); “Young 1000 Talent Plan” Program of China.

References

- [1] M. E. Fermann and I. Hartl, “Ultrafast fibre lasers,” *Nat. Photon.*, vol. 7, p. 868–874, 2013, <https://doi.org/10.1038/nphoton.2013.280>.
- [2] Y. Song, Z. Liang, X. Jiang, et al., “Few-layer antimonene decorated microfiber: ultra-short pulse generation and all-optical thresholding with enhanced long term stability,” *2D Mater.*, vol. 4, 2017, Art no. 045010, <https://doi.org/10.1088/2053-1583/aa87c1>.
- [3] M. Zhang, Q. Wu, F. Zhang, et al., “2D black phosphorus saturable absorbers for ultrafast photonics,” *Adv. Opt. Mater.*, vol. 7, 2018, Art no. 1800224, <https://doi.org/10.1002/adom.201800224>.
- [4] Y. Song, X. Shi, C. Wu, D. Tang, and H. Zhang, “Recent progress of study on optical solitons in fiber lasers,” *Appl. Phys. Rev.*, vol. 6, 2019, Art no. 021313, <https://doi.org/10.1063/1.5091811>.
- [5] S. T. Cundiff, B. C. Collings, N. N. Akhmediev, J. M. Soto-Crespo, K. Bergman, and W. H. Knox, “Observation of polarization-locked vector solitons in an optical fiber,” *Phys. Rev. Lett.*, vol. 82, p. 3988–3991, 1999, <https://doi.org/10.1103/PhysRevLett.82.3988>.
- [6] B. C. Collings, S. T. Cundiff, N. N. Akhmediev, J. M. Sotocrespo, K. Bergman, and W. H. Knox, “Polarization-locked temporal vector solitons in a fiber laser: experiment,” *J. Opt. Soc. Am. B*, vol. 17, p. 366–372, 2000, <https://doi.org/10.1364/JOSAB.17.000354>.
- [7] D. Y. Tang, H. Zhang, L. M. Zhao, N. Xiang, and X. Wu, “Soliton trapping in fiber lasers,” *Opt. Express*, vol. 16, p. 9528, 2008, <https://doi.org/10.1364/OE.16.009528>.
- [8] Y. Luo, J. Cheng, B. Liu, et al., “Group-velocity-locked vector soliton molecules in fiber lasers,” *Sci. Rep.*, vol. 7, p. 2369, 2017, <https://doi.org/10.1038/s41598-017-02482-w>.
- [9] M. Liu, A. P. Luo, Z. C. Luo, and W. C. Xu, “Dynamic trapping of a polarization rotation vector soliton in a fiber laser,” *Opt. Lett.*, vol. 42, p. 330–333, 2017, <https://doi.org/10.1364/OL.42.000330>.
- [10] L. M. Zhao, D. Y. Tang, H. Zhang, and X. Wu, “Polarization rotation locking of vector solitons in a fiber ring laser,” *Opt. Express*, vol. 16, p. 10053–10058, 2008, <https://doi.org/10.1364/oe.16.010053>.
- [11] H. Zhang, D. Tang, X. Wu, and L. Zhao, “Multi-wavelength dissipative soliton operation of an erbium-doped fiber laser,” *Opt. Express*, vol. 17, p. 12692–12697, 2009, <https://doi.org/10.1364/OE.22.011417>.
- [12] H. Zhang, D. Tang, L. Zhao, X. Wu, and H. Tam, “Dissipative vector solitons in a dispersion-managed cavity fiber laser with net positive cavity dispersion,” *Opt. Express*, vol. 17, p. 455–460, 2009, <https://doi.org/10.1364/OE.17.000455>.
- [13] K. Krupa, K. Nithyanandan, and P. Grelu, “Vector dynamics of incoherent dissipative optical solitons,” *Optica*, vol. 4, p. 1239, 2017, <https://doi.org/10.1364/optica.4.001239>.
- [14] H. Zhang, D. Tang, L. Zhao, Q. Bao, and K. P. Loh, “Vector dissipative solitons in graphene mode locked fiber lasers,” *Opt. Commun.*, vol. 283, p. 3334–3338, 2010, <https://doi.org/10.1016/j.optcom.2010.04.064>.
- [15] T. Habruseva, C. Mou, A. Rozhin, and S. V. Sergeev, “Polarization attractors in harmonic mode-locked fiber laser,” *Opt. Express*, vol. 22, p. 15211, 2014, <https://doi.org/10.1364/oe.22.015211>.
- [16] C. Mou, S. Sergeev, A. Rozhin, and S. Turistyn, “All-fiber polarization locked vector soliton laser using carbon nanotubes,” *Opt. Lett.*, vol. 36, p. 3831–3833, 2011, <https://doi.org/10.1364/OL.36.003831>.
- [17] S. V. Sergeev, C. Mou, A. Rozhin, and S. K. Turitsyn, “Vector solitons with locked and precessing states of polarization,” *Opt.*

- Express, vol. 20, p. 27434–27440, 2012, <https://doi.org/10.1364/OE.20.027434>.
- [18] C. Mou, S. V. Sergeev, A. G. Rozhin, and S. K. Turitsyn, “Bound state vector solitons with locked and precessing states of polarization,” *Opt. Express*, vol. 21, p. 26868–26875, 2013, <https://doi.org/10.1364/OE.21.026868>.
- [19] V. Tsaturian, S. V. Sergeev, C. Mou, et al., “Polarisation dynamics of vector soliton molecules in mode locked fibre laser,” *Sci. Rep.*, vol. 3, p. 3154, 2013, <https://doi.org/10.1038/srep03154>.
- [20] S. V. Sergeev, C. Mou, E. G. Turitsyna, A. Rozhin, S. K. Turitsyn, and K. Blow, “Spiral attractor created by vector solitons,” *Light Sci. Appl.*, vol. 3, p. e131, 2014, <https://doi.org/10.1038/lsa.2014.12>.
- [21] H. Khashi, S. V. Sergeev, C. Mou, et al., “Bright-dark rogue waves,” *Ann. Phys.*, vol. 530, 2018, Art no. 1700362, <https://doi.org/10.1002/andp.201700362>.
- [22] H. J. Khashi, S. V. Sergeev, M. A. Arami, N. Tarasov, and A. Rozhin, “Vector soliton rain,” *Laser Phys. Lett.*, vol. 16, 2019, Art no. 035103, <https://doi.org/10.1088/1612-202X/aaf89b>.
- [23] A. G. Rozhin, Y. Sakakibara, M. Tokumoto, H. Kataura, and Y. Achiba, “Near-infrared nonlinear optical properties of single-wall carbon nanotubes embedded in polymer film,” *Thin Solid Films*, vol. 464–465, p. 368–372, 2004, <https://doi.org/10.1016/j.tsf.2004.07.005>.
- [24] V. Scardaci, A. G. Rozhin, P. H. Tan, et al., “Carbon nanotubes for ultrafast photonics,” *Phys. Status Solidi B*, vol. 244, p. 4303–4307, 2007, <https://doi.org/10.1002/pssb.200776194>.
- [25] A. Jorio, A. G. Souza Filho, G. Dresselhaus, et al., “G-band resonant Raman study of 62 isolated single-wall carbon nanotubes,” *Phys. Rev. B*, vol. 65, 2002, <https://doi.org/10.1103/PhysRevB.65.155412>.
- [26] M. S. Dresselhaus, A. Jorio, A. G. Souza Filho, and R. Saito, “Defect characterization in graphene and carbon nanotubes using Raman spectroscopy,” *Philos. Trans. Ser A, Math. Phys. Eng. Sci.*, vol. 368, p. 5355–5377, 2010, <https://doi.org/10.1098/rsta.2010.0213>.
- [27] H. Kataura, Y. Kumazawa, Y. Maniwa, et al., “Optical properties of single-wall carbon nanotubes,” *Synth. Met.*, vol. 103, p. 2555–2558, 1999, [https://doi.org/10.1016/S0379-6779\(98\)00278-1](https://doi.org/10.1016/S0379-6779(98)00278-1).
- [28] M. Milnera, J. Kürti, M. Hulman, and H. Kuzmany, “Periodic resonance excitation and intertube interaction from quasicontinuous distributed helicities in single-wall carbon nanotubes,” *Phys. Rev. Lett.*, vol. 84, p. 1324, 2000, <https://doi.org/10.1103/PhysRevLett.84.1324>.
- [29] P. Grelu and N. Akhmediev, “Dissipative solitons for mode-locked lasers,” *Nat. Photon.*, vol. 6, p. 84–92, 2012, <https://doi.org/10.1038/nphoton.2011.345>.
- [30] S. Zhdanovich, A. A. Milner, C. Bloomquist, et al., “Control of molecular rotation with a chiral train of ultrashort pulses,” *Phys. Rev. Lett.*, vol. 107, 243004, 2011, <https://doi.org/10.1103/PhysRevLett.107.243004>.
- [31] B. Öktem, I. Pavlov, S. Ilday, et al., “Nonlinear laser lithography for indefinitely large-area nanostructuring with femtosecond pulses,” *Nat. Photon.*, vol. 7, p. 897–901, 2013, <https://doi.org/10.1038/nphoton.2013.272>.
- [32] Y. Jiang, T. Narushima, and H. Okamoto, “Nonlinear optical effects in trapping nanoparticles with femtosecond pulses,” *Nat. Phys.*, vol. 6, p. 1005–1009, 2010, <https://doi.org/10.1038/nphys1776>.
- [33] H. Yuan, X. Wang, B. Lian, et al., “Generation and electric control of spin-valley-coupled circular photogalvanic current in WSe₂,” *Nat. Nanotechnol.*, vol. 9, p. 851–857, 2014, <https://doi.org/10.1038/nnano.2014.183>.